Electronic Supplementary Information

Insights into Constitutional Isomeric Effects on Donor-Acceptor Intermolecular Arrangements in Non-fullerene Organic Solar Cells

Jungho Lee,[†a] Eun Min Go,[†b] Satej Dharmapurikar,[†a] Jianqiu Xu,[†c] Sang Myeon Lee,[a] Mingyu Jeong,[a] Kyu Cheol Lee,[a] Jiyeon Oh,[a] Yongjoon Cho,[a] Chunfeng Zhang,[c] Min Xiao,[c] Sang Kyu Kwak,*[b] and Changduk Yang*[a]

[a.] Department of Energy Engineering, School of Energy and Chemical Engineering, Perovtronics Research Center, Low Dimensional Carbon Materials Center, Ulsan National Institute of Science and Technology (UNIST), Ulsan 44919, Republic of Korea.

[b.] Department of Energy Engineering, School of Energy and Chemical Engineering, Ulsan National Institute of Science and Technology (UNIST), Ulsan 44919, Republic of Korea.

[c.] National Laboratory of Solid State Microstructures, School of Physics, and Collaborative Innovation Center of Advanced Microstructures, Nanjing University, Nanjing 210093, China.

*yang@unist.ac.kr; skkwak@unist.ac.kr

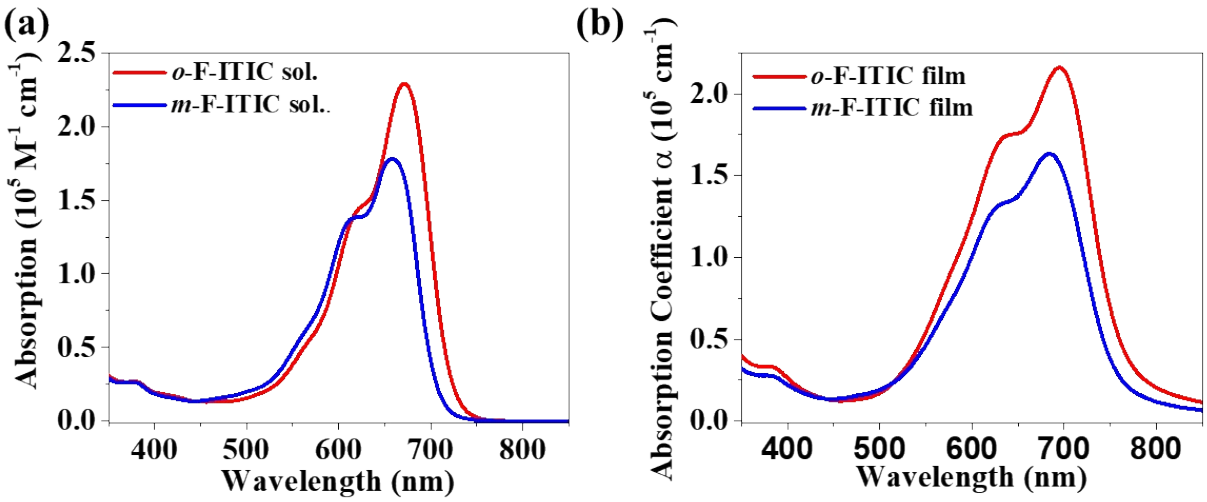

Fig. S1 Absorbance of the F-ITICs in (a) dilute chloroform solution and (b) films.

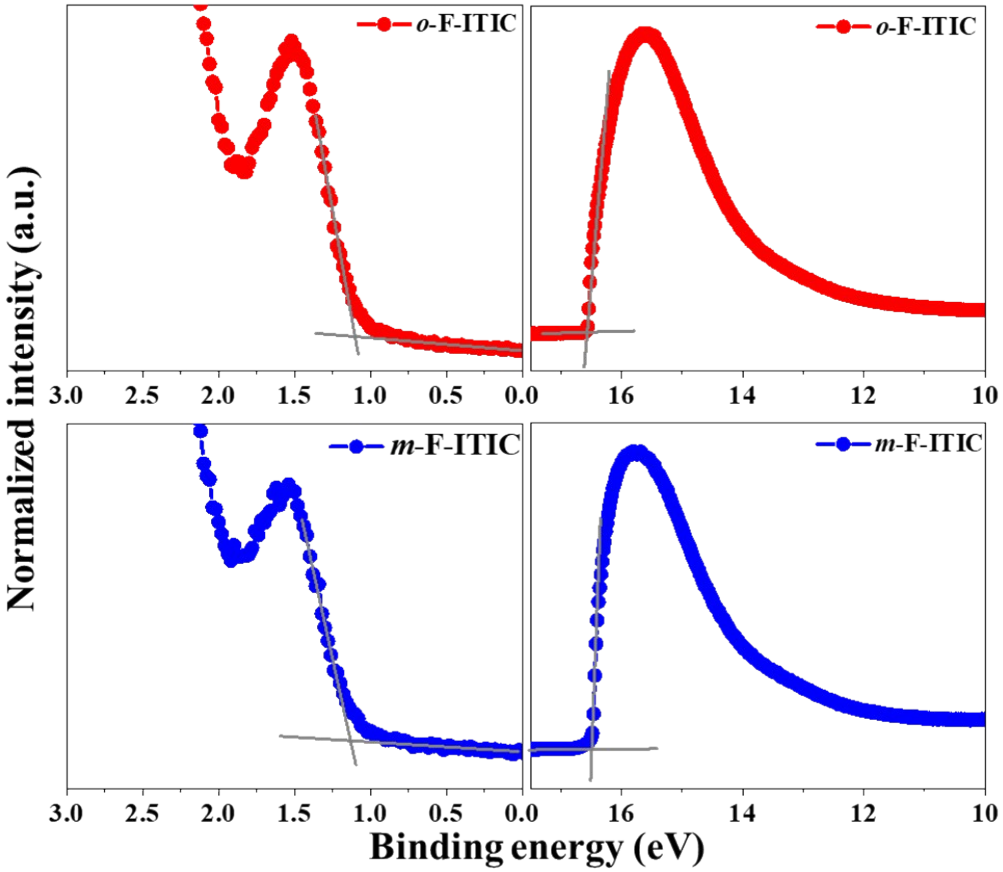

Fig. S2 Ultraviolet photoelectron spectra of *o*-F-ITIC and *m*-F-ITIC using HeI emission (*hv* =21.2 eV) as a light source. The calculated HOMO levels of *o*-F-ITIC and *m*-F-ITIC are -5.74 eV and -5.77 eV, respectively.

Table S1 Photovoltaic properties of the OSCs based on PBDB-T:*o*-F-ITIC with different D/A ratio.[a]

D/A ratio	V_{OC} [V]	J_{SC} [mA cm^{-2}]	*FF* [%]	PCE [%]
1:1	0.918	15.45	65.62	9.23 (9.42)
1.3:1	0.912	15.93	65.25	9.47 (9.65)
1.5:1	0.901	15.24	65.77	9.04 (9.20)
2:1	0.899	15.44	62.67	8.69 (8.97)

[a]The photovoltaic properties were averaged over eight devices and the maximum efficiencies were given in parentheses.

Table S2 Photovoltaic properties of the OSCs based on PBDB-T:*o*-F-ITIC (D/A; 1.3:1 wt%) with different amount of DIO additive.[a]

DIO contents	V_{OC} [V]	J_{SC} [mA cm^{-2}]	*FF* [%]	PCE [%]
0.5%	0.909	16.37	66.81	9.94 (10.03)
1%	0.909	16.24	62.08	9.16 (9.26)
2%	0.903	15.93	59.87	8.61 (9.12)

[a]The photovoltaic properties were averaged over eight devices and the maximum efficiencies were given in parentheses.

Table S3 Photovoltaic properties of the OSCs based on PBDB-T:*o*-F-ITIC (D/A; 1.3:1 wt%) containing 0.5 vol% of DIO with different annealing temperature.[a]

T °C	V_{OC} [V]	J_{SC} [mA cm^{-2}]	*FF* [%]	PCE [%]
60	0.912	17.65	67.30	10.83 (11.11)
100	0.910	17.27	66.22	10.40 (10.47)
140	0.909	16.93	65.76	10.12 (10.29)
180	0.894	16.29	61.61	8.96 (9.31)

[a]The photovoltaic properties were averaged over eight devices and the maximum efficiencies were given in parentheses.

Table S4 Photovoltaic properties of the OSCs based on PBDB-T:*m*-F-ITIC with different D/A ratio.[a]

D/A ratio	V_{OC} [V]	J_{SC} [mA cm^{-2}]	*FF* [%]	PCE [%]
1:1	0.884	14.34	59.32	7.51 (7.71)
1.3:1	0.880	14.61	60.46	7.77 (7.97)
1.5:1	0.875	14.41	59.84	7.55 (7.67)
2:1	0.849	14.10	50.26	6.02 (6.26)

[a]The photovoltaic properties were averaged over eight devices and the maximum efficiencies were given in parentheses.

Table S5 Photovoltaic properties of the OSCs based on PBDB-T:*m*-F-ITIC (D/A; 1.3:1 wt%) with different amount of DIO additive.[a]

DIO contents	V_{OC} [V]	J_{SC} [mA cm^{-2}]	*FF* [%]	PCE [%]
0.5%	0.881	15.19	60.66	8.12 (8.37)
1%	0.879	14.42	59.84	7.58 (7.96)
2%	0.869	14.24	56.04	6.93 (7.18)

[a]The photovoltaic properties were averaged over eight devices and the maximum efficiencies were given in parentheses.

Table S6 Photovoltaic properties of the OSCs based on PBDB-T:*m*-F-ITIC (D/A; 1.3:1 wt%) containing 0.5 vol% of DIO with different annealing temperature.[a]

T °C	V_{OC} [V]	J_{SC} [mA cm^{-2}]	*FF* [%]	PCE [%]
60	0.878	15.72	63.91	8.82 (8.90)
100	0.876	15.42	63.08	8.51 (8.62)
140	0.874	15.05	60.69	7.98 (8.44)
180	0.860	14.31	54.92	6.75 (6.84)

[a]The photovoltaic properties were averaged over eight devices and the maximum efficiencies were given in parentheses.

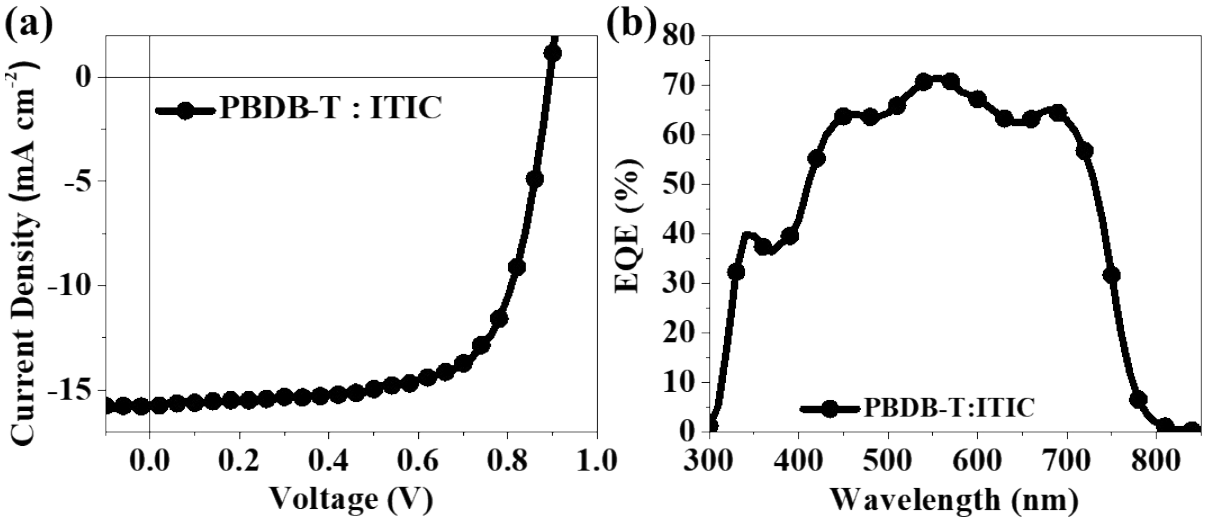

Fig. S3 (a) *J-V* curves of the device with PBDB-T:ITIC system and (b) the corresponding EQE curve.

Table S7 Photovoltaic properties of the OSCs based on PBDB-T:ITIC (D/A; 1:1 wt%) containing 0.5 vol% of DIO after thermal annealing treatment at 150 °C for 10 min.[a]

	V_{OC} [V]	J_{SC} [mA cm^{-2}]	*FF* [%]	PCE [%]
PBDB-T:ITIC	0.894	15.74	68.84	9.50 (9.69)

[a]The photovoltaic properties were averaged over eight devices and the maximum efficiencies were given in parentheses. [b]Obtained by integration of the EQE curves.

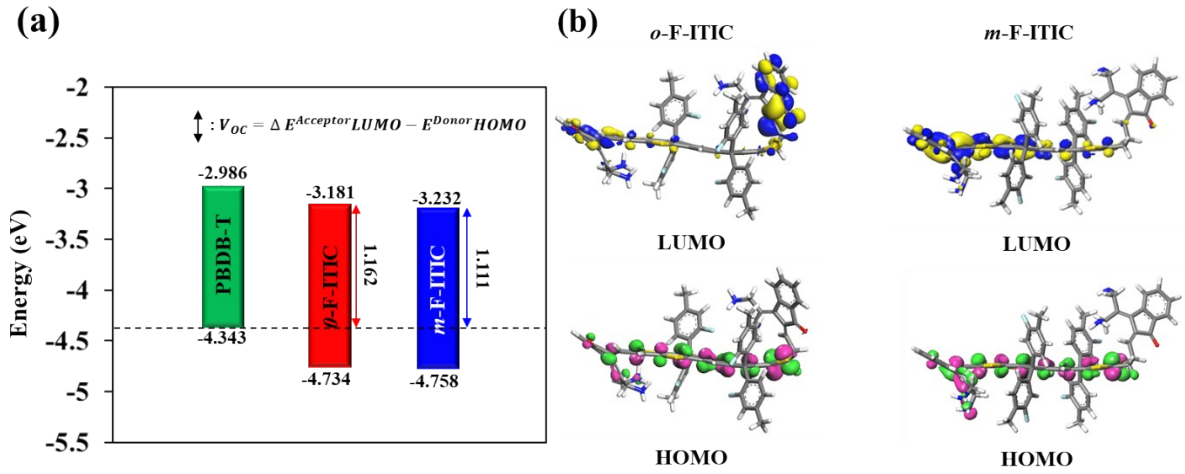

Fig. S4 (a) Energy diagram of the PBDB-T, *o*-F-ITIC, and *m*-F-ITIC. (b) Electron density distributions of HOMO and LUMO for optimized *o*-F-ITIC and *m*-F-ITIC. Gray, yellow and light blue represents carbon, sulfur and fluorine atoms, respectively.

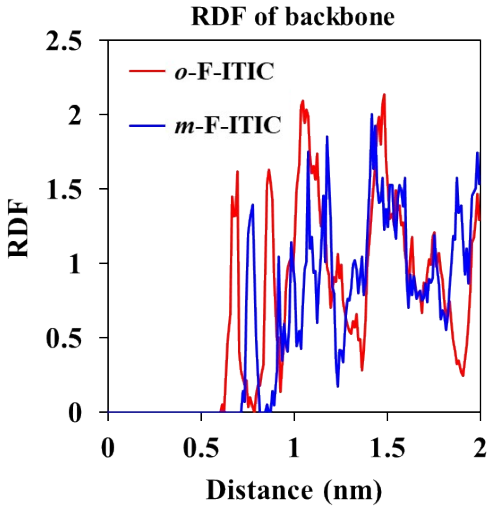

Fig. S5 Radial distribution function (RDF) of backbone of PBDB-T and F-ITICs.

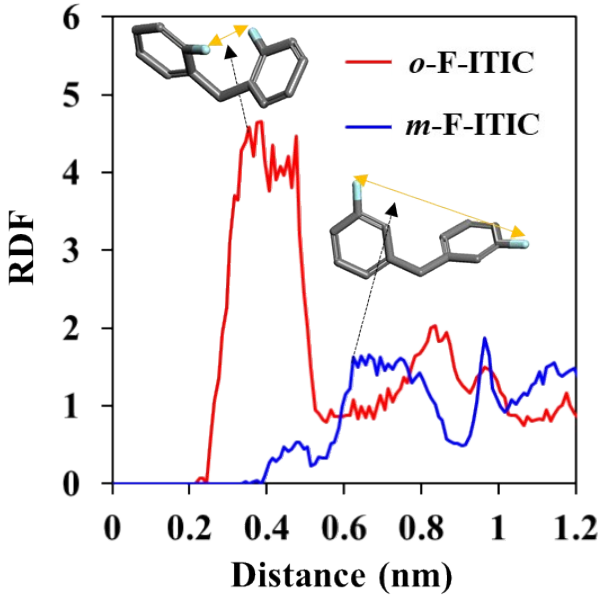

Fig. S6 RDF of fluorine atoms in *o*-F-ITIC and *m*-F-ITIC. Insets show the structure of fluorine atoms in *o*-F-ITIC and *m*-F-ITIC.

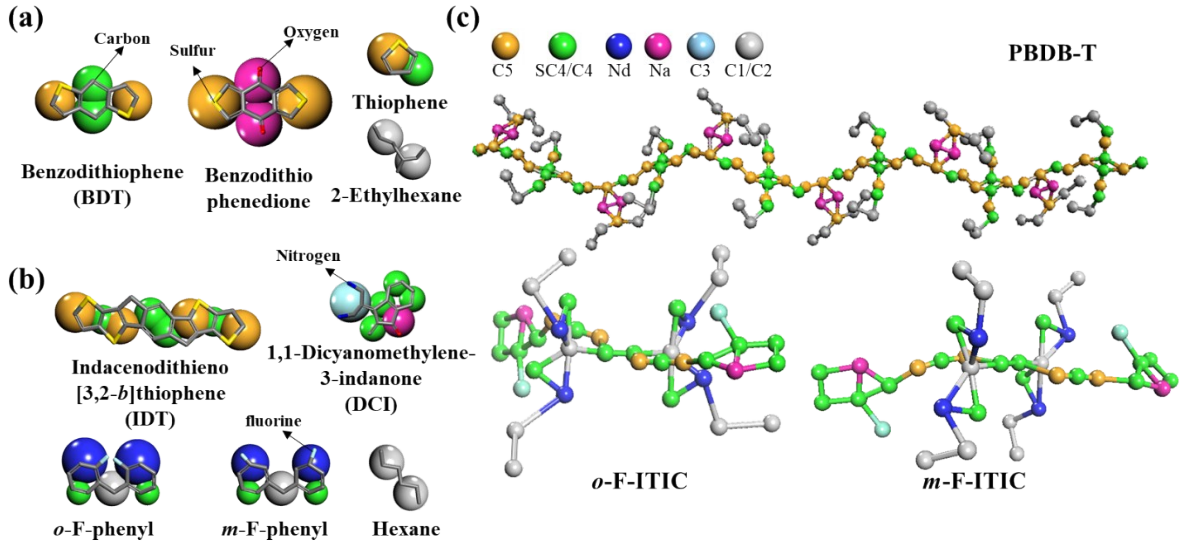

Fig. S7 Coarse-grained models of (a) PBDB-T and (b) F-ITICs. (c) PBDB-T and F-ITICs are shown with constituent CG beads. Martini bead types for CG beads are shown in the figure and hydrogen atoms are not shown in all atom model for clarity.

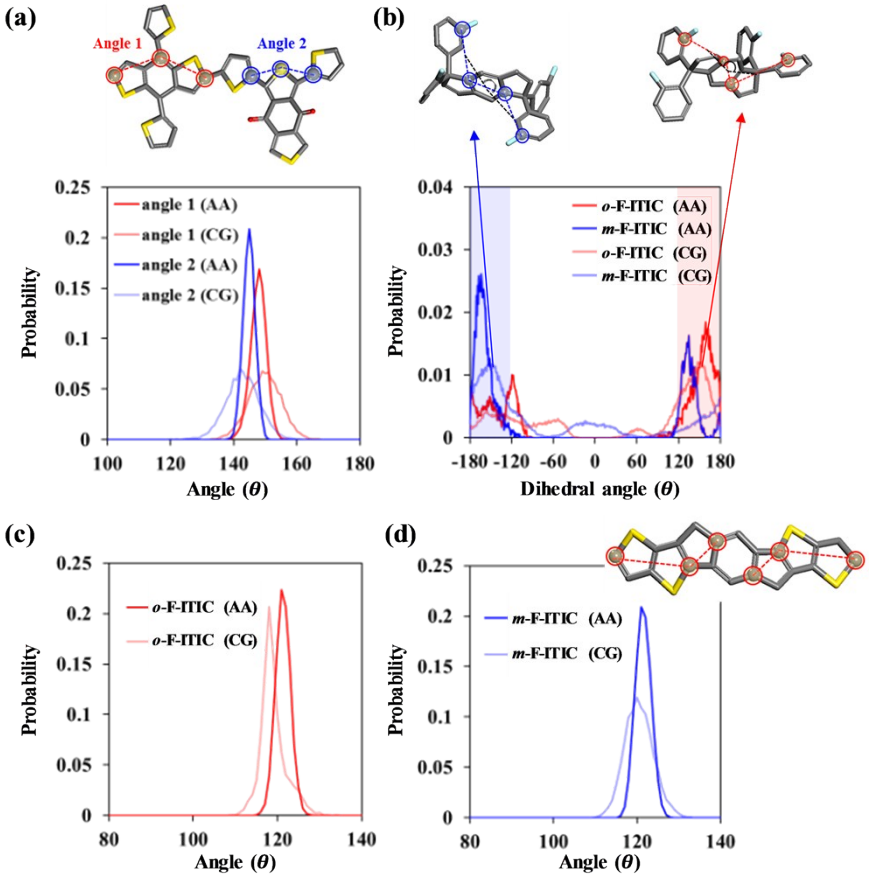

Fig. S8 (a) Probability distributions of angles in backbone of PBDB-T and angles are shown above the graph. (b) Probability distributions of dihedral angles of *o*-F-ITIC and *m*-F-ITIC. Insets show the dihedral angle. Probability distributions of angles in backbone of (c) *o*-F-ITIC and (d) *m*-F-ITIC. Angles are shown above the graph. AA and CG represent the results of all-atom and coarse-grained model, respectively.

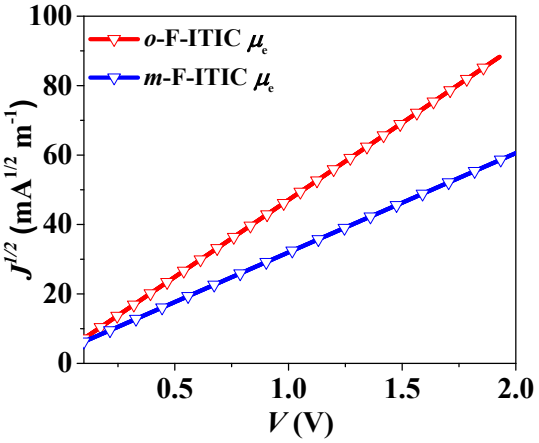

Fig. S9 Electron-only SCLC fittings of *o*-F-ITIC and *m*-F-ITIC neat films.

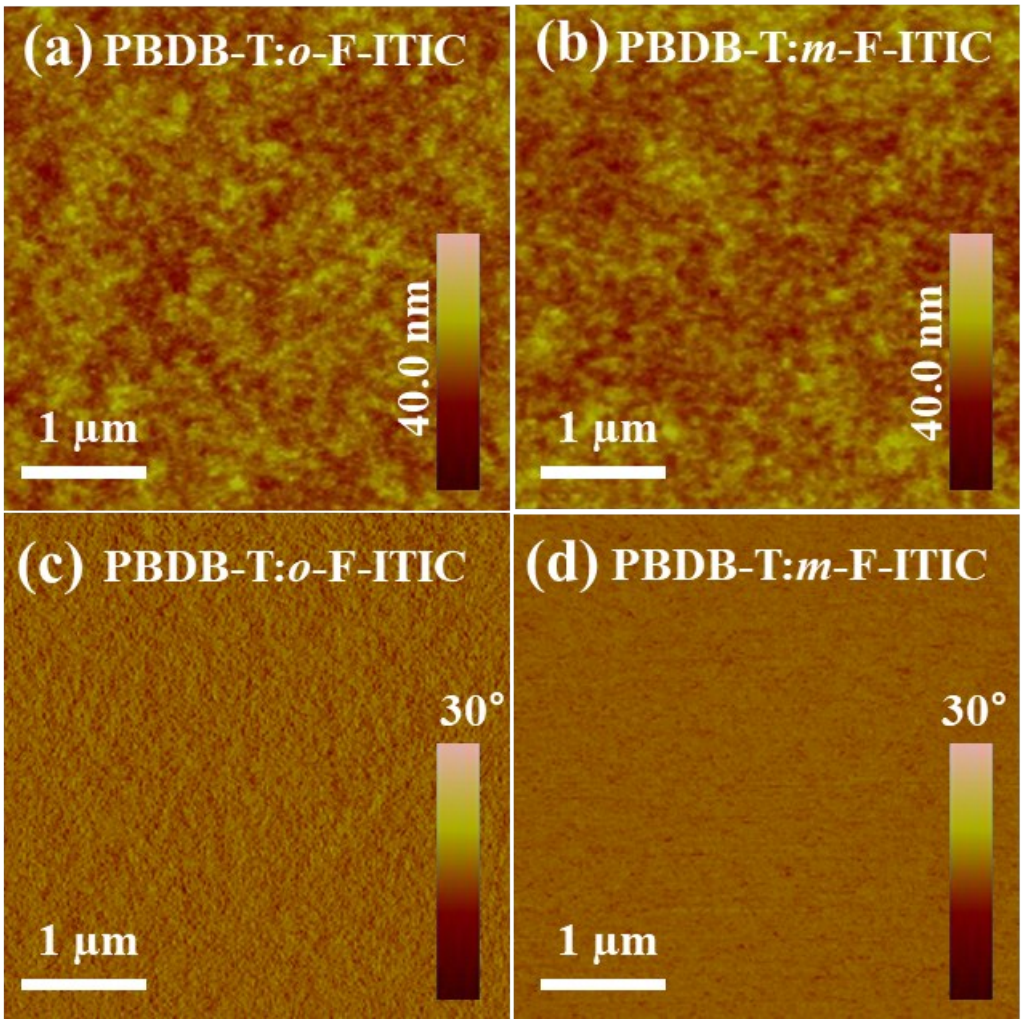

Fig. S10 AFM height and phase images with blend films composed of (a, c) PBDB-T:*o*-F-ITIC and (b, d) PBDB-T:*m*-F-ITIC, respectively.

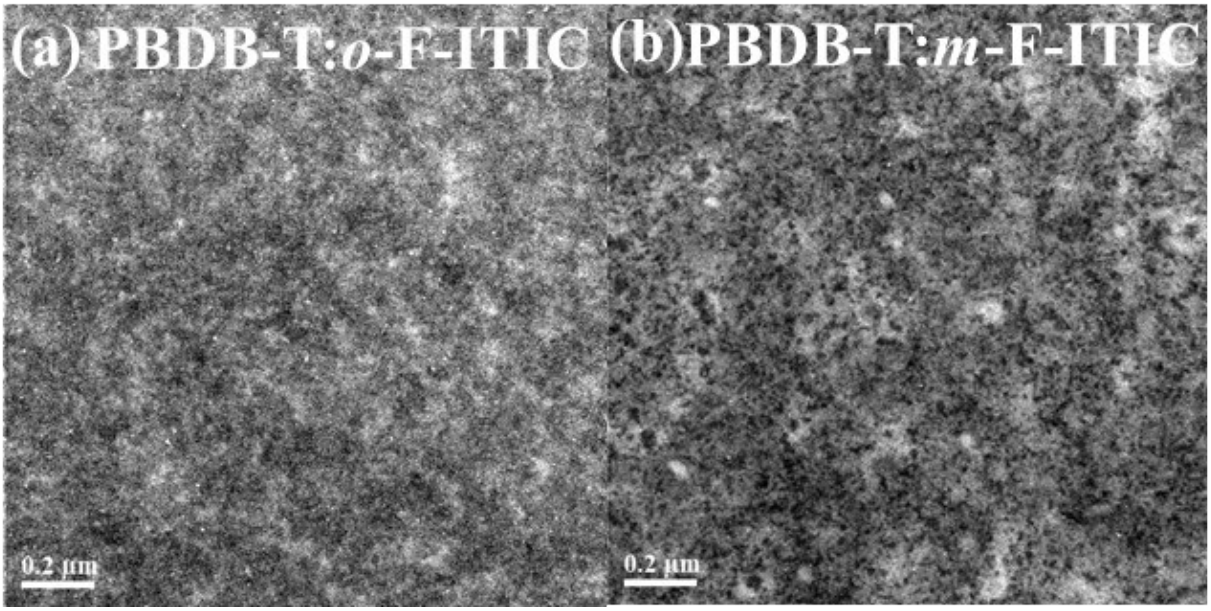

Fig. S11 STEM images with blend films composed of (a) PBDB-T:*o*-F-ITIC and (b) PBDB-T:*m*-F-ITIC, respectively.

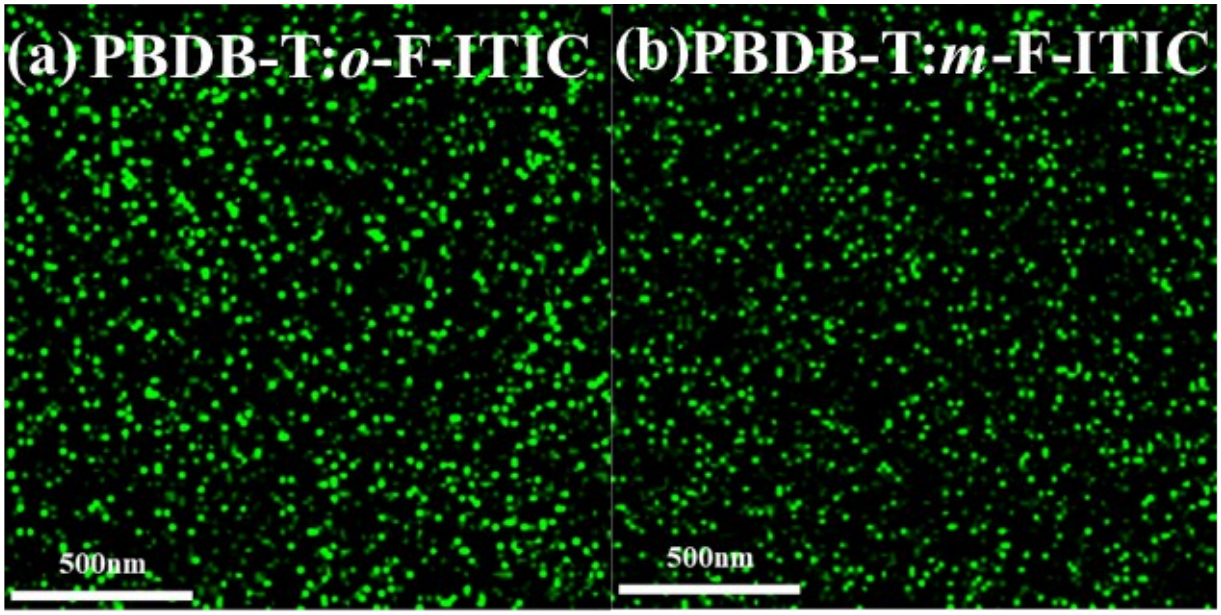

Fig. S12 EDAX eletmental mapping of fluorine element images with blend films composed of (a) PBDB-T:*o*-F-ITIC and (b) PBDB-T:*m*-F-ITIC, respectively.

Table S8 GIWAXS parameters of neat PBDB-T,*o*-F-ITIC, and *m*-F-ITIC films and blends of PBDB-T:*o*-F-ITIC and PBDB-T:*m*-F-ITIC films.

	q_{xy}			q_z		
	Lamellar stacking [Å]	π-π stacking [Å]	CCL (Lamellar peak) [nm]	Lamellar stacking [Å]	π-π stacking [Å]	CCL (π-π stacking) [nm]
PBDB-T	21.7	N/A	7.48	21.0	3.8	1.86
o-F-ITIC	19.8	N/A	5.18	N/A	3.6	2.14
m-F-ITIC	17.6	4.3	1.29	N/A	4.1	1.03
PBDB-T:*o*-F-ITIC	21.6	N/A	7.83	20.1	3.7	1.62
PBDB-T:*m*-F-ITIC	21.6	N/A	8.79	21.4	3.8	1.56

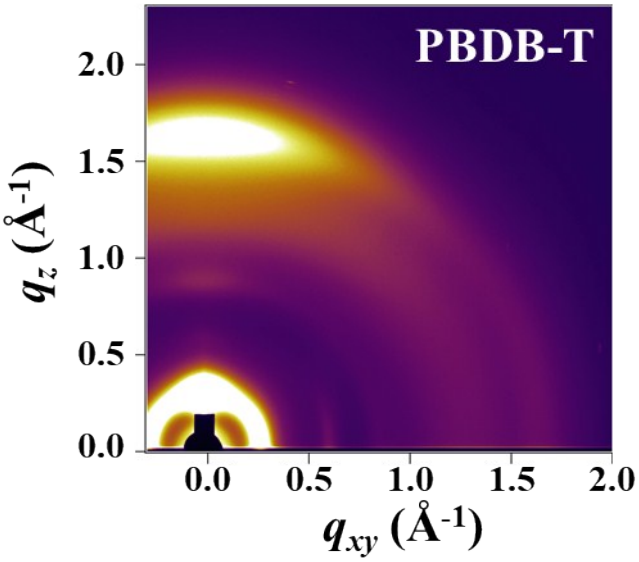

Fig. S13 2D GIWAXS images with neat films composed of PBDB-T.

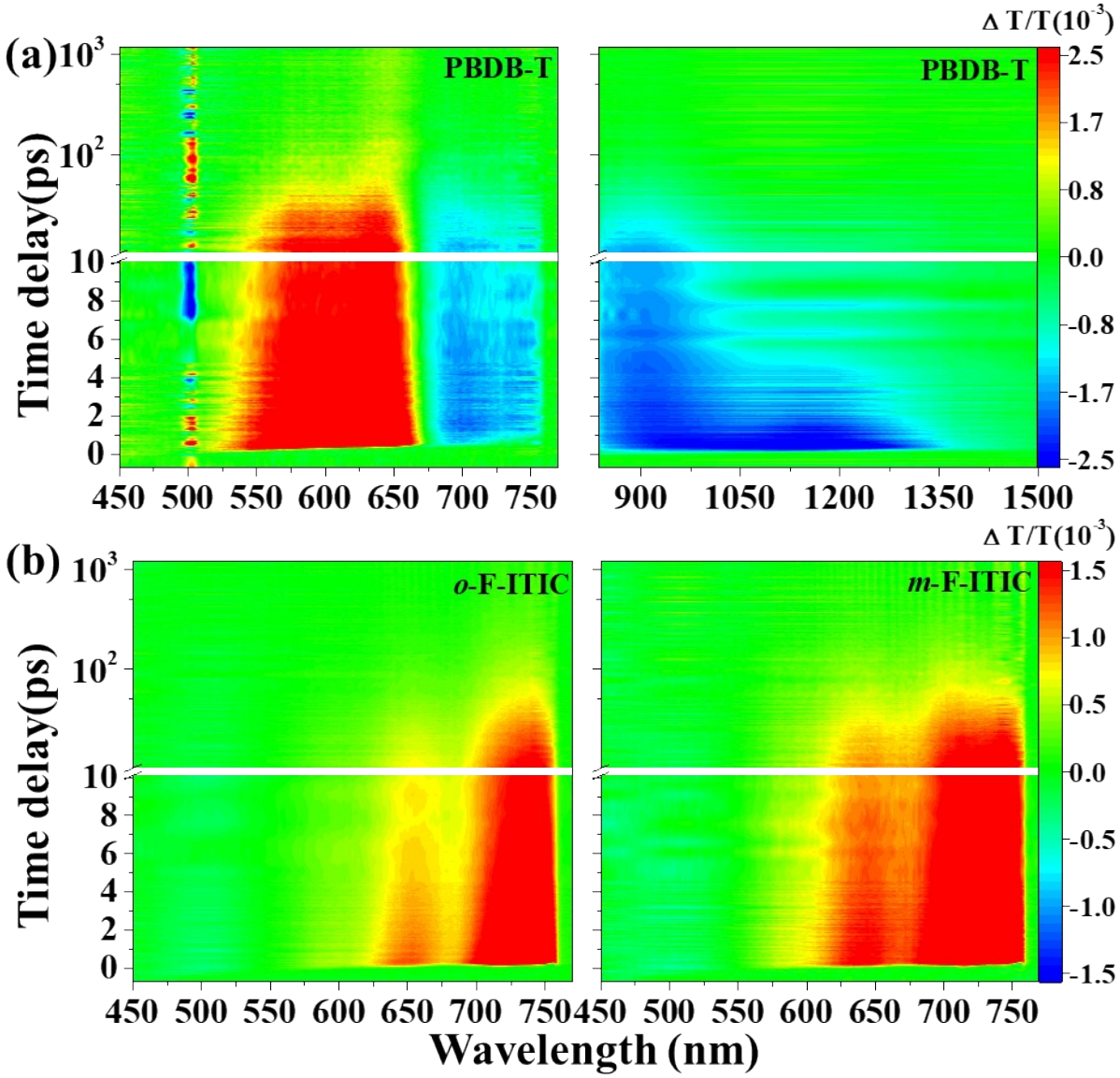

Fig. S14 TA signal recorded from (a) the neat film of PBDB-T excited by 500 nm and (b) the neat film of *o*-F-ITIC and *m*-F-ITIC excited by 710 nm.

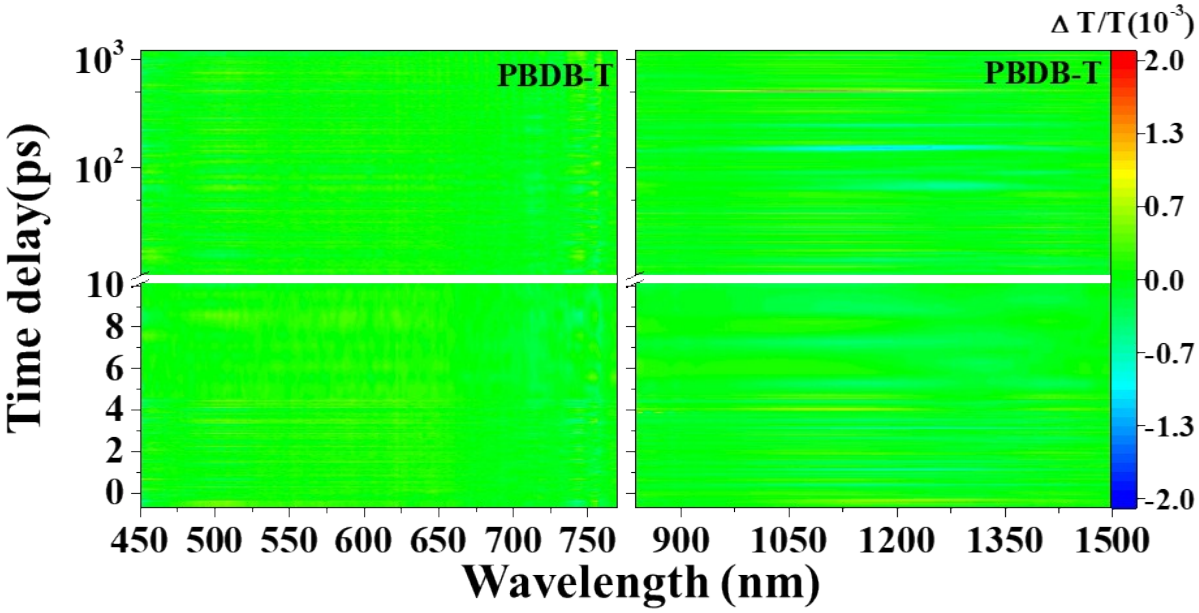

Fig. S15 TA signal recorded from the neat film of PBDB-T excited by 710 nm.

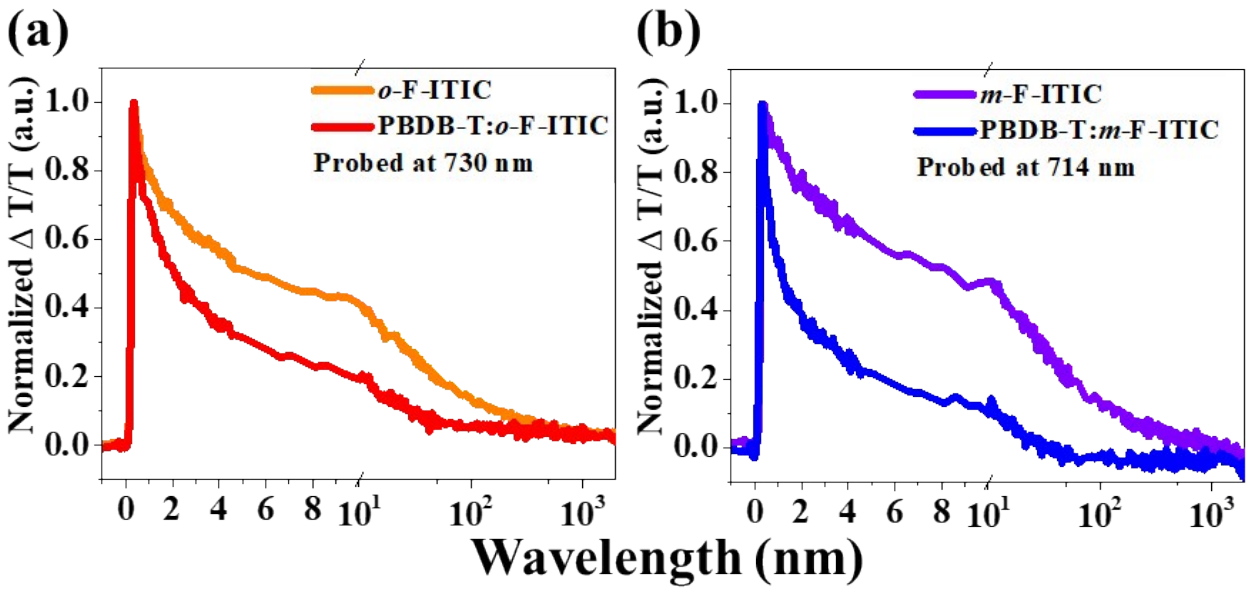

Fig. S16 TA dynamics (a) probed at 730 nm recorded from the films of neat *o*-F-ITIC and blend PBDB-T:*o*-F-ITIC and (b) probed at 714 nm recorded from the films of neat *m*-F-ITIC and blend PBDB-T:*m*-F-ITIC.